ON THE INFLUENCE OF BASE FLOW CHARACTERISTICS ON CROSSFLOW INSTABILITY IN SWEPT BOUNDARY LAYERS

Zhen-Ming Xu^{1,2,3}, Zhong-Hua Han^{1,2,3*}, Han Nie^{1,2,3} & Wen-Ping Song^{1,2,3}

¹School of Aeronautics, Northwestern Polytechnical University, Xi'an 710072, China
 ²National Key Laboratory of Aircraft Configuration Design, Xi'an 710072, China
 ³Institute of Aerodynamic and Multidisciplinary Design Optimization, Xi'an 710072, China

Abstract

Crossflow instability (CFI) is a critical factor contributing to the early transition of the boundary layer on highly swept wings. This paper investigates the influence of base flow characteristics on CFI in swept boundary layers, with a specific focus on the maximum crossflow velocity and the crossflow shape factor. Using linear stability theory, the development of stationary crossflow disturbances is analyzed. The results indicate that the maximum crossflow velocity linearly scales the nondimensional amplification rate in the unstable region of these disturbances. Additionally, variations in the crossflow shape factor impact the range of unstable wavenumbers and the critical Reynolds number. These findings are expected to provide valuable insights into developing strategies to mitigate crossflow instability.

Keywords: base flow, natural laminar flow, crossflow instability, linear stability theory

1. Introduction

In response to growing environmental concerns in aviation, the aeronautic community has set ambitious targets for energy savings and emission reductions targets in next-generation transport aircraft. Achieving these objectives requires the development of breakthrough technologies to significantly reduce aerodynamic drag [1]. One promising approach that has been extensively studied over the past decades is laminar flow technology. This technology holds significant potential for reducing viscous drag, which constitutes a major component of total drag on modern transport aircraft, typically accounting for over 50% on a transport aircraft such as the A320 [2].

The laminar-to-turbulent transition is driven by the growth of unstable disturbances in the three-dimensional boundary layer on a swept wing. Researches have identified four types of instabilities that cause transion [3]: streamwise (Tollmien-Schlichting instabilities in two-dimensional flows), crossflow, attachment line [4] and centrifugal [5]. Among them, crossflow instabilities (CFI) is a crucial factor that triggers early transition in the leading-edge regions on a swept wing. CFI is known to be a type of inviscid instability governed by the inflection point in the crossflow velocity profile, which results from the combination of wing sweep and pressure gradient. Reed and Saric [6, 7] and Saric et al. [3] have provided comprehensive reviews of CFI in three-dimensional boundary layers. Suppressing CFI has been challenging because of its formation mechanism. A favorable pressure gradient used to suppress Tollmien-Schlichting instabilities instead destabilizes CFI. Unfortunately, a strong favorable pressure gradient inevitably exists in the leading-edge area of a wing.

To suppress CFI and extend laminar flow, the concepts of natural laminar flow (NLF), laminar flow control (LFC), and hybrid laminar flow control (HLFC) are employed. NLF uses shape tailoring to modify the pressure gradient, thereby altering the base flow to suppress the growth of crossflow disturbances [8, 9]. LFC employs methods such as wall suction, plasma actuators [10], and discrete roughness elements (DRE) [2,7] to delay the transition process dominated by crossflow. HLFC combines the concepts of NLF and LFC to reduce system complexity and additional energy requirements [11]. Most of these strategies rely on tailoring base-flow velocity profiles to delay transition, highlighting the importance of understanding the influence of base-flow variations on the growth of crossflow disturbances.

This paper aims to investigate the impact of two key characteristics of base-flow velocity profiles on CFI: the maximum crossflow velocity and the crossflow shape factor. Two groups of crossflow velocity profiles are established based on Falkner-Skan-Cooke boundary layer, varying in maximum crossflow velocities and shape factors. The development of stationary crossflow disturbances in these boundary layers is analyzed using linear stability theory. Subsequently, the neutral curves and amplification rates are presented, and the influences of the maximum crossflow velocity and the crossflow shape factor are discussed.

This paper continues in Section 2 with the description of the stability analysis method. Section 3 provides a description of the base flow and crossflow velocity profiles. Section 4 presents the results and discussion of the stability analysis. Finally, Section 5 concludes the paper.

2. Numerical Method

Linear stability theory is used to analyze the development of crossflow disturbances. It is assumed that disturbances are small, and the flow is parallel. The three-dimensional small disturbance is described as

$$q'(x, y, z, t) = \hat{q}(y)e^{i(\alpha x + \beta z - \omega t)}$$
(1)

where $\hat{q}(y)$ is an amplitude function, α and β are wavenumbers in the x and z directions, respectively, and ω is the angular frequency. In spatial mode, α and β are regarded as complex numbers while ω is a real number. Then, Eq. (1) is written as

$$q'(x, y, z, t) = \hat{q}(y)e^{-(\alpha_i x + \beta_i z)}e^{i(\alpha_r x + \beta_r z - \omega_t)}$$
(2)

It demonstrates that when α_i or β_i is negative, the amplitude of disturbance grows along the x or z direction; when α_i or β_i is positive, the amplitude of disturbance decays along the x or z direction. Combine Eq. (2) with the Navier-Stokes equations, three-dimensional compressible linear stability equations are obtained.

The linear stability equations are high-order differential equations. They are translated into first-order differential equations during numerical computation, such as

$$\mathbf{Z}' = \mathbf{PZ} \tag{3}$$

The central difference and two-point averaging method are then used to discretize the first-order linear differential equations in the *y* direction as

$$-\left(\mathbf{I} + \frac{h_{j-1}}{2}\mathbf{P}\right)\mathbf{Z}_{j-1} + \left(\mathbf{I} - \frac{h_{j-1}}{2}\mathbf{P}\right)\mathbf{Z}_{j} = \mathbf{R}_{j} = 0$$
(4)

The homogeneous control equations and the homogeneous boundary conditions lead the equations to be solved as an eigenvalue problem. Replace one of the original homogeneous boundary conditions with a non-homogeneous boundary condition to enable the calculation of non-trivial solutions, and solve eigenvalues using Newton iteration method to satisfy the original boundary condition. Cebeci [12] provides a detailed description of the difference equations and the numerical method.

In spatial mode, there are six eigenvalues $(\alpha_r, \alpha_i, \beta_r, \beta_i, \omega, Re)$. Given any four parameters, the remaining two parameters can be determined by eigenvalue equations. The eigenvalue equations are originating from the original homogeneous boundary condition as

$$F\left(\alpha_r, \alpha_i, \beta_r, \beta_i, \omega, Re\right) = 0 \tag{5}$$

In the field of complex numbers, Eq. (5) represents two equations. In this paper, Mack/Arnal relation is used where β_r is assumed to be zero.

An in-house code is developed to carry out the process of solving the linear stability equations and obtain the development of stationary CF disturbances in linear stage [13–16]. The reason for considering only the linear stage is that the research by Reed et al. [17] has demonstrated that suppressing disturbances in this stage, where disturbances are small and weak, is most effective.

3. Crossflow Velocity Profiles

3.1 Characteristics of Crossflow Velocity Profiles

Crossflow is caused by the imbalance of centripetal acceleration and pressure gradient within a boundary layer. Outside the boundary layer, inviscid streamlines are curved because of wing sweep and pressure gradient where a balance is existed. Inside the boundary, the pressure gradient exceeds the centripetal acceleration because of the effects of viscous. As a result, velocity profiles inside the boundary layer are distorted. The component of the distorted velocity profile in the direction normal to the inviscid streamline is the crossflow velocity profile. Figure 1 provides a typical crossflow velocity profile and the definition of maximum crossflow velocity w_m and crossflow shape factor H_c . The height δ_{cf} is the height at which the crossflow is 10% of the maximum value, while y_m is the height at which the crossflow velocity reaches its maximum value. The crossflow shape factor is defined as the ratio of these two heights as

$$H_c = \frac{y_m}{\delta_{cf}} \tag{6}$$

These two factors related to the properties of inflection points which are the source of CFI. They have influences on critical Reynolds number, range of unstable wave number and growth rate of crossflow disturbances.

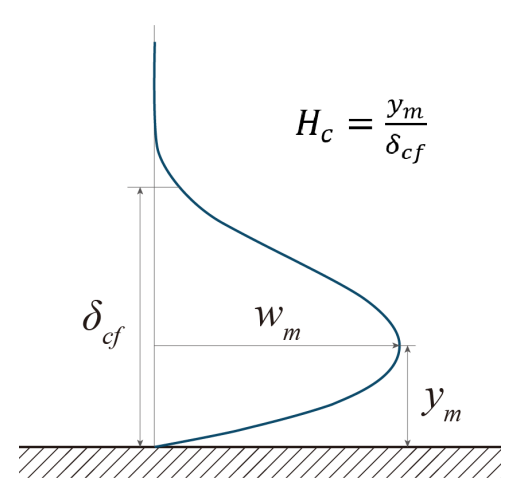


Figure 1 – Definition of maximum crossflow velocity and crossflow shape factor.

3.2 Base Flow

Before investigating the characteristics of crossflow velocity profiles, it is necessary to create a base flow. The Falkner-Skan-Cooke (FSC) boundary layer is a suitable choice for this purpose, as its crossflow velocity profiles can be obtained parametrically. For the FSC boundary layer, the components of the inviscid flow at the outer edge in the chordwise and spanwise directions are denoted as u_e and w_e , respectively, which are

$$u_e = c(x_c)^m$$

$$w_e = \text{const.}$$
(7)

In this flow, the pressure gradient exists only in the chordwise direction, and the velocity in the spanwise direction is constant. The boundary-layer equations for the FSC boundary layer, as shown by Cooke [18], are

$$f'''(\eta) + \frac{1}{2}(m+1)f(\eta)f''(\eta) + m(1 - f'^{2}(\eta)) = 0$$

$$g''(\eta) + \frac{1}{2}(m+1)f(\eta)g'(\eta) = 0$$
(8)

where η is the dimensionless normal distance perpendicular to the wall surface, defined as

$$\eta = \sqrt{\frac{u_e}{v_e x_c}} y \tag{9}$$

By solving Eq. (8), dimensionless velocity profiles in the chordwise and spanwise directions can be obtained

$$u_c(\eta) = \frac{u_c(\eta)}{u_e} = f'(\eta)$$

$$w_s(\eta) = \frac{w_s(\eta)}{w_e} = g(\eta)$$
(10)

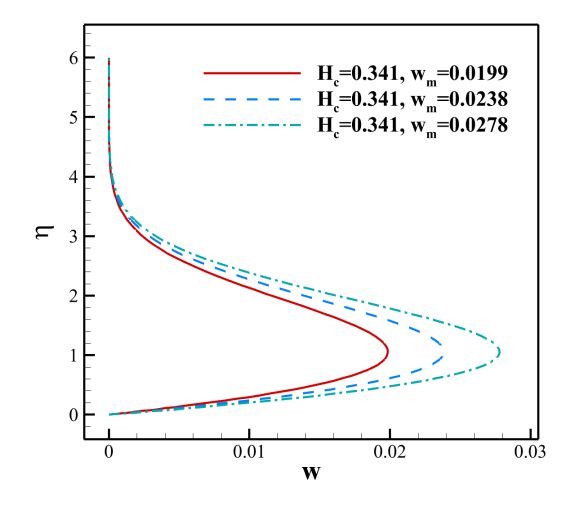
The dimensionless streamwise and crossflow velocity profiles u and w with respect to the local potential velocity $q_e = \sqrt{u_e^2 + w_e^2}$ are given by

$$u(\eta) = f'(\eta)\cos^2\theta + g(\eta)\sin^2\theta$$

$$w(\eta) = \left[-f'(\eta) + g(\eta)\right]\cos\theta\sin\theta$$
(11)

where θ is the angle between the direction of the local inviscid flow and the chordwise direction.

In the following study, two groups of crossflow velocity profiles are generated based on the FSC boundary layer, with each group containing three profiles. The first group is used to study the effects of maximum velocity, as shown in Figure 2. The three crossflow velocity profiles have the same shape factor, but their maximum velocities differ by factors of 1.2 and 1.4, respectively. The second group is used to study the effects of crossflow shape factor, as shown in Figure 3. The three crossflow velocity profiles share the same maximum velocity, but differ in their shape factors. In both groups, the crossflow velocity profile represented by the red line serves as the baseline, corresponding to the conditions of m = 0.05, $\theta = 30 \deg$. Additionally, the streamwise velocity profiles are kept the same as in the baseline condition (m = 0.05, $\theta = 30 \deg$) for all cases.



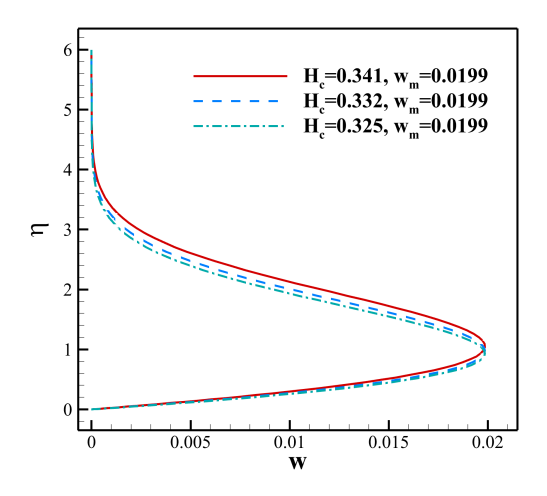


Figure 2 – Crossflow velocity profiles used to study the effects of maximum velocity.

Figure 3 – Crossflow velocity profiles used to study the effects of shape factor

4. Results and Discussion

In this section, the results of the linear stability analysis for the aforementioned two groups of velocity profiles are presented. The effects of maximum crossflow velocity and crossflow shape factor on the stability characteristics of stationary crossflow disturbances are presented and discussed.

4.1 Effects of maximum velocity

The group with different maximum crossflow velocities is the first to be investigated. Their stability characteristics are calculated using the method mentioned in section 2. The specified eigenvalues in this calculation are frequency $\omega_r=0$, nondimensional spanwise wave number β_r , and the local Reynolds number Re, where Re is based on the local potential velocity q_e and the reference length $L=\sqrt{V_ex_c/u_e}$.

The spatial amplification rates for stationary crossflow disturbances for these velocity profiles is shown in Figure 4. The blue lines represent the neutral curves, while the orange dashed lines mark the positions of the critical Reynolds numbers Re_{cr} , which are 958, 799, and 685 for these crossflow velocity profiles. It can be observed that Re_{cr} decreases with the increase in maximum crossflow velocity. Furthermore, the critical Reynolds numbers differ by factors of 1.2 and 1.4, which are identical to the corresponding differences in crossflow velocities. The findings indicate that the maximum crossflow velocity linearly scales the critical Reynolds number.

To verify whether these findings are effective across the entire neutral curve, Figure 5 presents a comparison of the neutral curves. Additionally, the critical Reynolds numbers for $\beta_r = 0.15$, 0.45 and 0.70 are compared in Table 1. It can be observed that the shapes of neutral curves are similar, and the Reynolds numbers decrease as the maximum crossflow velocities increase. The Reynolds numbers corresponding to the same nondimensional wavenumber on the neutral curves are scaled by factors of 1.2 and 1.4 relative to the baseline (red solid line), which follows the same relationship as their maximum crossflow velocities. Therefore, the maximum crossflow velocity has a linear scaling effect on the Reynolds numbers along the neutral curve. If the maximum crossflow velocity is increased by a factor of k, the Reynolds numbers on the neutral curve will decrease by a factor of k.

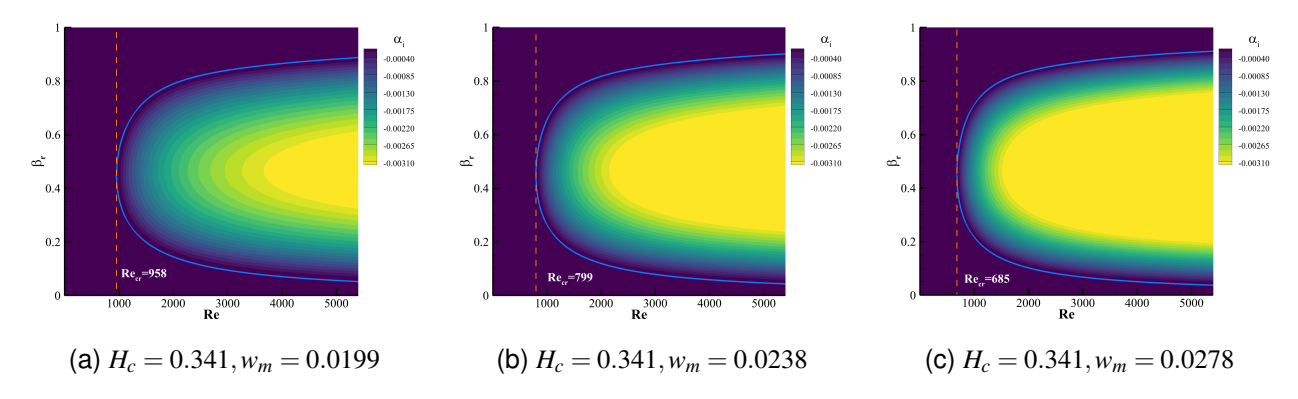


Figure 4 – Nondimensional spatial amplification rates for stationary crossflow disturbances at different maximum crossflow velocities.

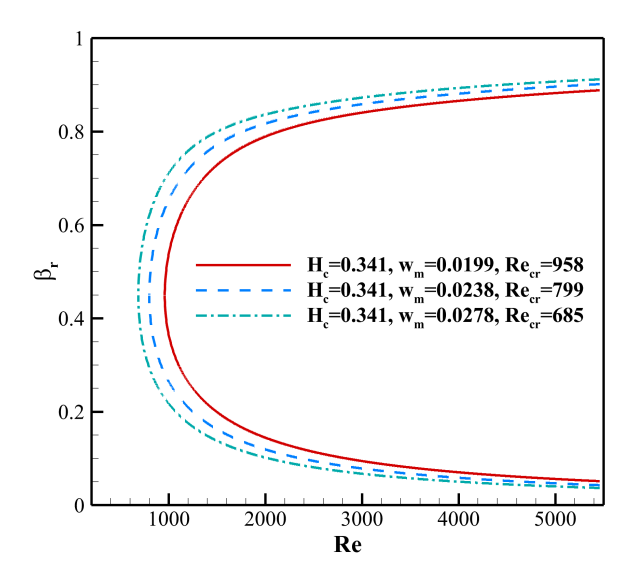


Figure 5 – Neutral curves for stationary crossflow disturbances at different maximum crossflow velocities.

Figure 6 compares the nondimensional amplification rates of these crossflow velocities at $\beta_r=0.5$, highlighting the scaling effect of maximum crossflow velocity on the nondimensional amplification rates. As shown in Figure 6, the absolute value of the amplification rates increases with the rise in maximum crossflow velocity. Moreover, a comparison of the amplification rates at Reynolds numbers Re=3000, Re=2500, and Re=2143, which are identical before being scaled by the maximum crossflow velocities, reveals that the amplification rates are also scaled by factors of 1.2 and 1.4, consistent with the maximum crossflow velocities.

From the above results, it can be concluded that the maximum crossflow velocity has a linear scaling effect on the Reynolds number and the nondimensional amplification rate in the unstable region of stationary crossflow disturbances. It is negatively correlated with the Reynolds number and positively correlated with the nondimensional amplification rate.

Table 1 – Comparison of Reynolds numbers on neutral curves with different maximum crossflow velocities at nondimensional wave numbers of 0.15, 0.45 and 0.70 ($H_c = 0.341$).

| | $w_m = 0.0199$ | $w_m = 0.0238$ | $w_m = 0.0278$ |
|------------------|----------------|----------------|----------------|
| $\beta_r = 0.15$ | 1932 | 1613 | 1385 |
| $\beta_r = 0.45$ | 958 | 799 | 685 |
| $\beta_r = 0.70$ | 1361 | 1130 | 966 |

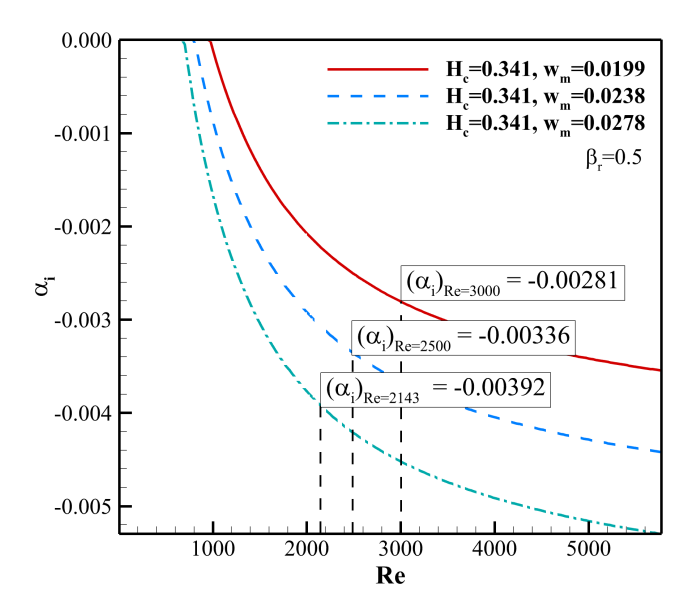


Figure 6 – Nondimensional amplification rate curves for stationary crossflow disturbances at different maximum crossflow velocities.

4.2 Effects of crossflow shape factor

The stability characteristics of the second group of velocity profiles with different crossflow shape factors are calculated using the same method as the first group. The contour plots of spatial amplification rates for stationary crossflow disturbances are shown in Figure 7. It can be seen that the decrease in the crossflow shape factor leads to the increase in the critical Reynolds number. The trend is consistent with the results obtained by Dagenhart [19]. In addition, Figure 7 reveals the increasing trend of the nondimensional amplification rate as the shape factor decreases.

As observed in Figure 8, the range of nondimensional wave numbers on the neutral curve changes as the variations of the crossflow shape factor, expecially on the upper branch. The range of β_r expands and the critical Reynolds number increases on the neutral curve as H_c decreases.

Figure 9 presents the amplification rates for nondimensional wavenumbers of 0.4 and 0.5. Although the disturbance becomes unstable earlier when the shape factor is larger, its amplification rate (absolute value) is smaller in the later stages.

In summary, the crossflow shape factor has effects on the range of the unstable region for crossflow stationary disturbances, leading to changes to the critical Reynolds number, the range of nondimensional wavenumbers, and the amplification rates.

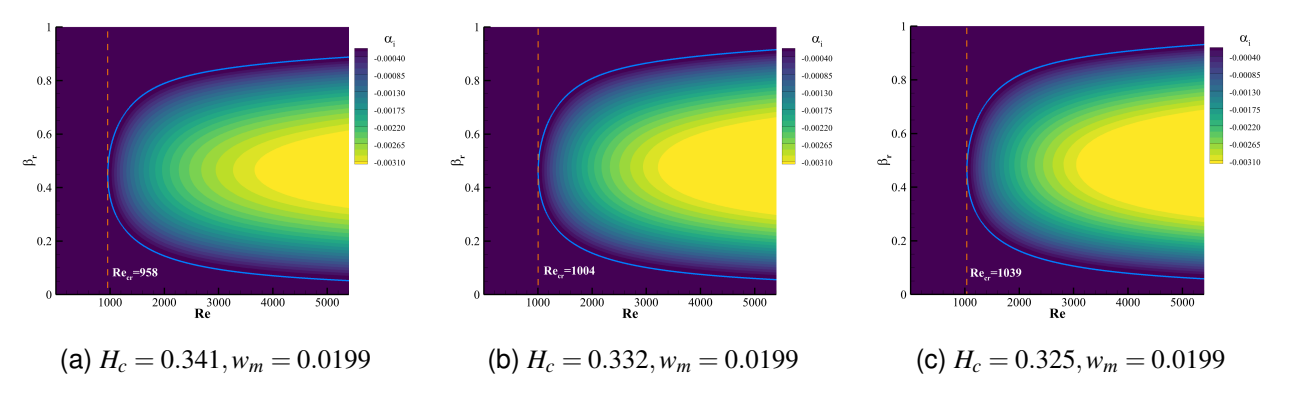


Figure 7 – Nondimensional spatial amplification rates for stationary crossflow disturbances at different crossflow shape factors.

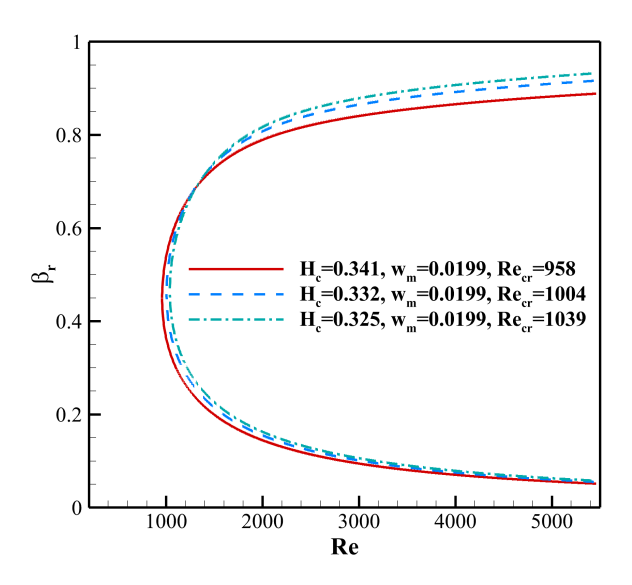


Figure 8 – Neutral curves for stationary crossflow disturbances at different crossflow shape factors.

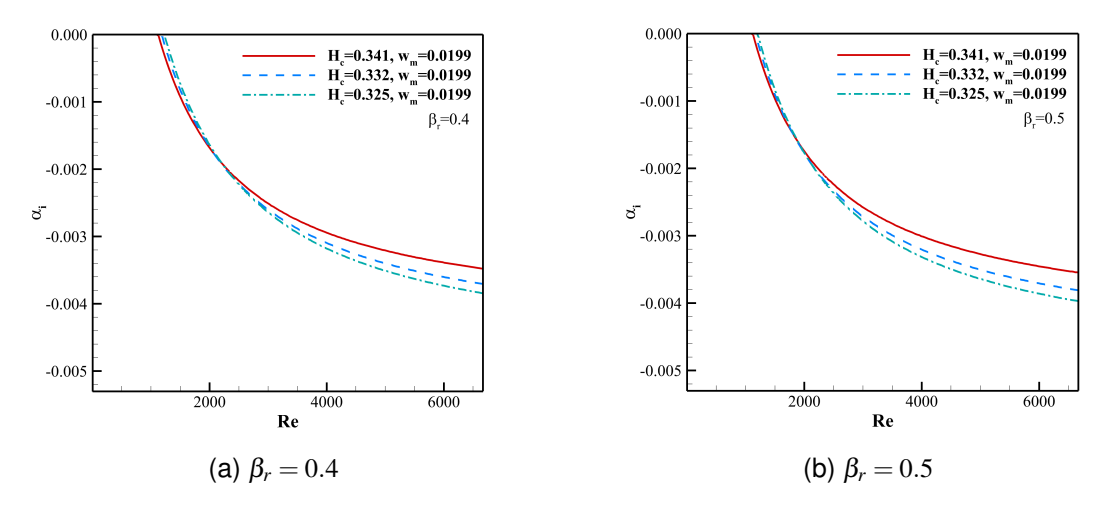


Figure 9 – Amplification rate curves for stationary crossflow disturbances at at different crossflow shape factors.

5. Conclusions

In the present paper, a detailed analysis of the effects of maximum crossflow velocity and crossflow shape factor on the stability characteristics of stationary crossflow disturbances is performed using linear stability theory. The results reveal that the maximum crossflow velocity has a linear scaling effect on the Reynolds number and nondimensional amplification rate, demonstrating that higher maximum crossflow velocities lead to increased CFI. Additionally, a decrease in the crossflow shape factor expands the range of unstable nondimensional wavenumbers and shifts the critical Reynolds number to higher values. These findings emphasize the importance of precisely controlling base flow characteristics to manage CFI effectively. Future research could focus on developing control strategies for CFI by tailoring base flow profiles based on the insights provided in this study.

6. Acknowledgement

This work was supported by the National Key Research and Development Program of China under Grant No. 2023YFB3002800, the National Natural Science Foundation of China (No. 12072285), and the Youth Innovation Team of Shaanxi Universities.

7. Contact Author Email Address

Zhong-Hua Han, Professor, hanzh@nwpu.edu.cn, Corresponding author.

8. Copyright Statement

The authors confirm that they, and/or their company or organization, hold copyright on all of the original material included in this paper. The authors also confirm that they have obtained permission, from the copyright holder of any third party material included in this paper, to publish it as part of their paper. The authors confirm that they give permission, or have obtained permission from the copyright holder of this paper, for the publication and distribution of this paper as part of the ICAS proceedings or as individual off-prints from the proceedings.

References

- [1] Abbas A, de Vicente J, and Valero E. Aerodynamic technologies to improve aircraft performance. *Aerospace Science and Technology*, Vol 28, No. 1, pp 100–132, 2013.
- [2] Saric W S, Carpenter A L, and Reed H L. Passive control of transition in three-dimensional boundary layers, with emphasis on discrete roughness elements. *Philosophical Transactions of The Royal Society A-mathematical Physical and Engineering Sciences*, Vol 369, No. 1940, pp 1352–1364, 2011.
- [3] Saric W S, Reed H L, and White E B. Stability and transition of three-dimensional boundary layers. *Annual Review of Fluid Mechanics*, Vol 35, No. 1, pp 413–440, 2003.
- [4] Poll D. Transition in the infinite swept attachment line boundary layer. *Aeronautical Quarterly*, Vol 30, No. 4, pp 607–629, 1979.
- [5] Saric W S. Görtler vortices. Annual Review of Fluid Mechanics, Vol 26, No. 1, pp 379-409, 1994.
- [6] Reed H L and Saric W S. Stability of three-dimensional boundary layers. *Annual Review of Fluid Mechanics*, Vol 21, No. 1, pp 235–284, 1989.
- [7] Saric W and Reed H. Crossflow instabilities theory & technology. 41st Aerospace Sciences Meeting and Exhibit, Reno, Nevada, 2003.
- [8] Campbell R L and Lynde M N. Natural laminar flow design for wings with moderate sweep. *34th AIAA Applied Aerodynamics Conference*, Washington, D.C., 2016.
- [9] Lynde M N, Campbell R L, Hiller B R, and Owens L R. Design of a crossflow attenuated natural laminar flow flight test article. *AIAA Scitech 2021 Forum*, VIRTUAL EVENT, 2021.
- [10] Yadala S, Hehner M T, Serpieri J, Benard N, Dörr P C, Kloker M J, and Kotsonis M. Experimental control of swept-wing transition through base-flow modification by plasma actuators. *Journal of Fluid Mechanics*, Vol 844, pp R2, 2018.

EFFECTS OF BASE FLOW CHARACTERISTICS ON CFI

- [11] Joslin R D. Aircraft laminar flow control. Annual Review of Fluid Mechanics, Vol 30, No. 1, pp 1–29, 1998.
- [12] Cebeci T. Stability and Transition: Theory and Application: Efficient Numerical Methods with Computer Programs. Horizons Pub., Long Beach, Calif., 1st edition, 2004.
- [13] Zhang K and Song W. Infinite swept-wing reynolds-averaged navier-stokes computations with full en transition criterion. *Proceedings of the 27th International Congress of the Aeronautical Sciences*, Nice, France, 2010.
- [14] Han Z H, Chen J, Zhang K S, Xu Z M, Zhu Z, and Song W P. Aerodynamic shape optimization of natural-laminar-flow wing using surrogate-based approach. *AIAA Journal*, Vol 56, No. 7, pp 2579–2593, 2018.
- [15] Xu Z M, Han Z H, Chi J B, Zhen Z, and Song W P. Crossflow instability analysis for swept laminar flow wings using crossflow pressure gradient. *AIAA Journal*, Vol 59, No. 8, pp 1–12, 2021.
- [16] Nie H, Song W, Han Z, Chen J, and Tu G. A surrogate-based en method for compressible boundary-layer transition prediction. *Journal of Aircraft*, Vol 59, No. 1, pp 89–102, 2022.
- [17] Reed H L, Saric W S, and Arnal D. Linear stability theory applied to boundary layers. *Annual Review of Fluid Mechanics*, Vol 28, No. 1, pp 389–428, 1996.
- [18] Cooke J C and Hall M. Boundary layers in three dimensions. *Progress in Aerospace Sciences*, Vol 2, No. 2, pp 222–282, 1962.
- [19] Dagenhart J R. Amplified crossflow disturbances in the laminar boundary layer on swept wings with suction. Technical Publication (TP) NASA-TP-1902, NASA, 1981.